Focusing Control under Microscopic Views based on Regional Monotones of Image Focal Values

Ku Chin Lin
Mechanical Engineering Department, Kun Shan University, 71003 Taiwan
kclin@mail.ksu.edu.tw

Abstract- **Generally, clarity of images or focal value (FV) varies in hill-shaped manner with respect to lens motion in a focus region. However, the FV variation in the far-off focused region is usually subjected to disturbances and the image signals may not be informative for focusing control. Therefore, challenges exist if focusing control under microscopic views for a large depth of lens displacement is needed. The challenges are primarily due to lack of a method to differentiate image FVs at far-off focused regions.**

This paper proposes a method to integrate regional monotones of FV variation. A focusing control algorithm with step-size adaptation is derived based on the above monotonous properties to gain speed and reliability. Information about the regional monotones is acquired and used for checking and correcting inconsistency in the motion direction of lens caused by image disturbances. This inconsistency check is significant on enhancing the robustness of focusing control.

Four case studies are illustrated to demonstrate the feasibility of the proposed algorithm and the effects of design parameters. A response time of 0.6~1.2 sec with perfect reliability is achieved. This speed is relatively sufficient for many industrial applications, such as LCD panel laser repairs.

I. INTRODUCTION

Auto focusing (AF) is a useful technique in many applications of photoelectric semiconductor, electronic manufacturing, biotechnology, mechatronics, and nano-technology. The technique has been implemented into a chip-embedded system, mobile phone CCD, and many industrial applications to ensure good imaging quality for measurement, inspection or servo control [1-5].

An AF technique could require a measure of quantifying the clarity of image in terms of a focal value (FV). One of such FV measures was developed by Choi *et al.* using the weighted median filtering for noise rejection [6]. Besides, the Wavelet and Discrete Cosine transforms were found to be able to attenuate noises [7, 8], Chebyshev moment was applied to overcome lighting variations [9], and adaptive thresholding was implemented in an FPGA-based AF system [10]. However, low illumination could induce a problem of low signal-to-noise (S/N) ratio for FV measure as images are far-off focus under a microscopic view. An advanced scheme is needed as a solution [11].

Many of the previous FV methods were developed based on (1) the image gradient, such as Tenengrad and Laplacian (2) the image moment, such as absolute central moment (ACM) and high-pass filtered image (3) the image variance such as variance of gray level (4) the image transformation such as fast Fourier transform and fast cosine transform [12, 13]. The methods are adequate as an FV measure for images of near-focus where the S/N ratio is normally high. However, for images far off focused where the illumination and the S/N ratio are normally low, the methods could become inadequate. As a result, most of the previous FV measures couldn't prove to be efficient under microscopic views of far-off-focus. In this study, a new FV measure for a large depth of lens displacement is presented.

Since a maximal (or, minimal) FV normally occurs at focus, the hill climbing search (HCS) algorithm was implemented to locate the maximum [14]. The algorithm may be comprised of multiple stages for the search and multiple steps of lens move in a fixed or adaptive step size [15]. The step size is a critical parameter for design in a microscopic AF control system. A proper step size is correlated with the depth of field (DOF) under different lens of magnification and it must be designated to achieve good robustness and speed of response. Wang *et al.* [16] studied focusing control to drive a robot arm under a microscopic lens of x3 magnification. The depth to drive the arm in the view is within $\pm 40\delta$ where δ denotes the DOF. However, problems of low S/N ratio could become significant as the depth to drive or the magnification of lens increases.

At near-focus, image FV normally varies in a hill-shaped manner. At far-off-focus, a secondary maximum of FV was observed in x50 microscopic views of liquid crystal display (LCD) [17]. The LCD images are shown in Fig. 1 where the lens position corresponding to the highest image FV is denoted by z=0. A hill shape of FV is obvious at a near-focus region (NFR). However, using a previous FV method, a secondary maximum could exist at a far-off-focus region (FFR) as it is shown at $z=45\delta$ in Fig. 2. This may cause a problem for the HCS control.

In this study, a new FV method of integrating regional monotonous variation of FV is proposed. Section II illustrates some typical FV measures and introduces the integration of the measures. With the integrating measure, an AF control algorithm with step-size adaptation is developed in Section III. In Section IV, the adequacy of the proposed algorithm is verified by experiment on an LCD AF system. Finally, the conclusions of this study are given in Section V.

II. INTEGRATION OF REGIONAL MONOTONES OF PREVIOUS FV MEASURES

The Tenengrad measure is one of the previous measures and it can be described below:

$$M_{Ten} = \frac{1}{N}\sum_{x,y}^{N} \left(\left|w_x * f(x,y)\right| + \left|w_y * f(x,y)\right|\right) \quad (1)$$

where $f(x,y)$ denotes image intensity at (x,y), N the total number of pixels in an image frame, the symbol "*" denotes a weighting-sum operator, $w_x = \begin{bmatrix} -1 & 0 & 1 \\ -2 & 0 & 2 \\ -1 & 0 & 1 \end{bmatrix}$, and $w_y = \begin{bmatrix} -1 & -2 & -1 \\ 0 & 0 & 0 \\ 1 & 2 & 1 \end{bmatrix}$.

The ACM measure is another and it can be described below:

$$M_{Acm} = \sum_{k=0}^{L-1} \left|k - \bar{f}\right| h(k), \quad (2)$$

where L denotes the number of image gray levels, $\bar{f}$ and $h(k)$ the mean intensity and histogram of image, respectively.

The variance of the Tenengrad measures of sub-windowing images is defined below:

$$M_{VTen} = \frac{1}{n-1}\sum_{ij} (m_{Ten,ij} - \overline{m}_{Ten})^2 \quad (3)$$

where $m_{Ten,ij} = \frac{1}{N_{ij}}\sum_{x,y} \left(\left|w_x * f_{ij}(x,y)\right| + \left|w_y * f_{ij}(x,y)\right|\right)$, $\overline{m}_{Ten} = \frac{1}{n}\sum_{ij} m_{Ten,ij}$, n denotes the number of sub-windows, the subscript i and j refer to the i^{th}-row and j^{th}-column of the sub-windows defined within the image scene.

The variance of the ACM measure of sub-windowing images is defined below:

$$M_{VAcm} = \frac{1}{n-1}\sum_{ij} (m_{Acm,ij} - \overline{m}_{Acm})^2 \quad (4)$$

where $m_{Acm,ij} = \sum_{k} \left|k - \bar{f}_{ij}\right| h_{ij}(k)$ and $\overline{m}_{Acm} = \frac{1}{n}\sum_{ij} m_{Acm,ij}$.

Shown in Fig. 3 is an example of variation of FVs without dimension over a NFR and FFRs. For each of the measures, the dimensionless FVs are defined by dividing the measure values by their maximum. At the FFR, when image features become less apparent, M_{Ten} and M_{Acm} are dominated by image noises, and so are for each of the sub-windowing measures. However, the corresponding variance measures will diminish in strength if the noises of the sub-windowing images have similar variance.

Compared with the measures M_{Ten} and M_{Acm}, the variance measures M_{VTen} and M_{VAcm} could have higher sensitivity to image clarity at the NFR and lower sensitivity to noise at the FFR. These phenomena were observed from comprehensive experiments [17]. The higher the sensitivity at the NFR is advantageous to AF control accuracy. The lower the sensitivity at the FFR is advantageous to thresholding an FFR from a NFR and to integrating the measure with another.

In this study, two measures are proposed for such integration. They are the mean of ensemble image intensity and the variance of sub-windowing image intensity as below:

$$M_{Int} = \bar{f} \quad (5)$$

$$M_{VInt} = \frac{1}{n-1}\sum_{ij} (\bar{f}_{ij} - \bar{\bar{f}}_{ij})^2 \quad (6)$$

where $\bar{\bar{f}}_{ij} = \frac{1}{n}\sum_{ij} \bar{f}_{ij}$.

Figure 4 shows schematic of LCD glass under focusing where the target object for focusing is the circuit layer embedded in an LCD glass. Typical target images are already given in Fig. 1. The images possess higher intensity than those of the background. In Fig. 4, z_4 denotes a well-focused lens position, z_1 the nearest position of lens could be moved to the target and z_8 the farthest position of lens could be moved away from the target.

Under ideally focused, an object point has a point image. The point image will spread outward and become a blur circle when it is not focused. The higher the degree of the out-of-focus is, the larger the diameter of the blur circle is.

The intensity measure M_{int} is mainly determined by two optical mechanisms. One is governed by the growth of the image blur. When image is slightly off focused, the blur circles are small in diameter as the case shown in Fig. 1(c). The mean intensity could increase as the image points with higher intensity expand within the view. However, as more and more the blur circles grow out of the view, the mean intensity will start to drop until a lowest level. This mechanism is independent of the direction of loss of focus as sketched by M_1 in Fig. 5. The other mechanism is due to the structure of the LCD panel and the microscopic lighting strategy. Since the target layer can absorb fraction of light, the images possess lower intensity at lens positions between z_1 and z_4 (*i.e.*, the darker side) than between z_4 and z_8 (*i.e.*, the brighter side). The fact of different image intensities at the two sides can be also observed from Fig. 1. From z_1 to z_8, the mean intensity increases monotonously at the darker side and then starts to decrease at some point in the brighter side as many of the blur circles grow out of the view. This intensity variation is sketched by M_2 in Fig. 5. The sum of M_1 and M_2 determines the measure M_{Int}.

The variation of M_{Vint} is also governed by the growth of the image blur and it has the same properties as that of the measure M_1. However, the former is more sensitive to the blur growth and to the image noises as well. However, the later effects could induce non-monotonous variation of M_{Vint} at the FFRs. Examples of the measures M_{Int}, M_{VInt} and M_{VAcm} for LCD images are given in Fig. 6. The measures have different regional monotonous variations which can be integrated and merged into a composite measure to expand the applicability for a wider range of lens displacement.

The measures can be divided into regional monotones by the direction of lens displacement, the FV variation and thresholding. First, the NFR is dividable from an FFR by introducing a threshold to the measure M_{VAcm} (say, t_{VAcm}) as shown by the horizontal dashed line in Fig. 6. Then, the NFR can be further divided into two regional monotones (*i.e.*, $z_3 \rightarrow z_4$ and $z_4 \rightarrow z_5$) by the direction of lens displacement and the FV increment or decrement. The FFRs can be divided into 5 regional monotones as shown by the vertical dashed lines in Fig. 6. Note that each of the 5 FFRs are dividable based on the direction of lens displacement and the variations of M_{Int}

and M_{VInt}, except $z_5 \rightarrow z_6$ and $z_1 \rightarrow z_2$. However, as the region $z_5 \rightarrow z_6$ is of the brighter side, the intensity is normally higher than that of the other. The two regions can be differentiated by introduce a threshold to the measure M_{Int} as shown in Fig. 6.

The schemes of the above dividing process into 7 regional monotones are summarized in Table 1. The same schemes are also applicable and expandable if a wider range of lens displacement is needed.

III. PROPOSED AF ALGORITHM BASED ON REGIONAL MONOTONES

The proposed focusing algorithm is composed of three stages which are determination of initial direction, rough tuning, and fine tuning, respectively. A flowchart of the proposed focusing control algorithm is given in Fig. 7.

The initial step size is designed depending on the width of the NFR which is fixed for a specific lens and can be measured by experiment. If the lens is initially at the NFR, one tenth of the width is used as the step size. If the lens is initially at the FFR, one third of the width is used. The former step size is appropriately small for not generating too large overshoot while the later is appropriately large for not generating instability.

The initial direction of lens displacement is determined by comparing the mean intensity of the current image with that of the focused image in the previous run. If the mean intensity of the current image is larger than that of the previous image, the current lens position is more probably at the brighter side. Then, move the lens toward the target by letting $\Delta z < 0$); otherwise move the lens away from the target by letting $\Delta z > 0$. However, improper initial direction determined above will be corrected in the next stage for rough tuning.

The rough tuning starts right after an initial lens displacement. Adaptative step size is implemented and the following rules are proposed for the adaptation:

If $M_{VAcm} < t_{VAcm}$, then

$$\Delta z_s = g_1 \delta,\ g_1 = \alpha\left(\frac{M_{VAcm}}{2t_{VAcm} - M_{VAcm}}\right)^{-\gamma}, \text{ and}$$
$$g_1 \le g_{\max} \tag{7.1}$$

If $M_{VAcm} \geqq t_{VAcm}$ and $\Delta M_{VAcm} > 0$, then

$$\Delta z_s = g_2 \delta,\ g_2 = \alpha\left(\frac{M_{VAcm}}{t_{VAcm}}\right)^{-\gamma}, \text{ and}$$
$$g_{\min} \le g_2 \le g_{\max} \tag{7.2}$$

where $\alpha > 0$ and $\gamma > 0$.

The step size is parameterized in terms of DOF. It is a multiplier of the DOF described by the gains g_1 and g_2 for the FFR and NFR, respectively. Each gain is designated as a power function with a negative power and a positive multiplier. The power and the multiplier can be designated of different values at different NFR and FFR regions. The gains should be properly bounded. A lower bound can be set to avoid too small a step size for gaining the speed. An upper bound can be set to avoid abnormal influence of impulse noise for ensuring stability.

Typical lower bounds for the gain g_2 can be 0.2~0.5. A too small lower bound could be inappropriate as it could result in undifferentiated FV changes in a lens displacement. On the other hand, at the FFR, a larger step size is used to gain the speed as the lens positions is farther off focus. Nonetheless, too large a step size could result in a large overshoot or instability. For this reason, at the FFR, the upper bound for g_2 should be never greater than the width of the NFR. In this study, one third of the width seems to be appropriate for setting the upper bound for g_2.

The direction of lens displacement during rough tuning is determined by the following rules:

If $M_{VAcm,s-1} < t_{VAcm}$ and $\Delta M_{Int,s-1}\Delta M_{VIn,s-1} > 0$, then
$\Delta z_s \Delta z_{s-1} \Delta M_{VInt,s-1} > 0$. (8.1)

If $M_{VAcm,s-1} < t_{VAcm}$, $\Delta z_{s-1}\Delta M_{Int,s-1} < 0$ and
$\Delta z_{s-1}\Delta M_{VInt,s-1} > 0$, then $\Delta z_s < 0$. (8.2)

If $M_{VAcm,s-1} < t_{VAcm}$, $\Delta z_{s-1}\Delta M_{Int,s-1} > 0$, $\Delta z_{s-1}\Delta M_{VInt,s-1} < 0$, then
If $M_{Int,s-1} \geqq t_{Int}$, then $\Delta z_s < 0$, otherwise $\Delta z_s > 0$. (8.3)

If $M_{VAcm,s-1} \geqq t_{VAcm}$ and $\Delta z_{s-1}\Delta M_{VAcm,s-1} > 0$, then
$\Delta z_s \Delta z_{s-1} > 0$. (8.4)

If $M_{VAcm,s-1} \geqq t_{VAcm}$ and $\Delta z_{s-1}\Delta M_{VAcm,s-1} < 0$, then
$\Delta z_s \Delta z_{s-1} < 0$. (8.5)

where s denotes an iteration index for rough tuning.

The above rules are developed based on the monotonous variations of measures in Table 1. By Eq. (8.1), if $M_{VAcm,s-1} < t_{VAcm}$ and $\Delta M_{Int,s-1}\Delta M_{VInt,s-1} > 0$, then the lens position at the previous iteration could be at the region of $z_2 \rightarrow z_3$ or $z_6 \rightarrow z_7$. If the lens position is at $z_2 \rightarrow z_3$, then as a consequence of Eq. (8.1), we have $\Delta z_{s-1}\Delta M_{VInt,s-1} > 0$ and $\Delta z_s > 0$; the lens is to be moved away from the target at the current iteration. If the lens position is at $z_6 \rightarrow z_7$, then $\Delta z_{s-1}\Delta M_{VInt,s,s-1} < 0$ and $\Delta z_s < 0$; the lens will be moved toward the target at the current iteration. Similar explanations hold for the other rules of Eqs (8).

If the initial direction of lens displacement was incorrect or pulse-noises took effects, inconsistency of lens displacement could occur during the focusing control at the FFR. Inconsistency arises when a lens displacement is not heading toward focus at any focusing searching. To enhance the robustness of the focusing control, checks for such inconsistency are proposed. Conditions of inconsistency have been developed based on the Table 1 and are summarized below:

$\Delta M_{Int,s-1} < 0$ and $\Delta M_{VInt,s-1} < 0$. (9.1)

$\Delta z_{s-1}\Delta M_{Int,s-1} > 0$, $\Delta z_{s-1}\Delta M_{VInt,s-1} < 0$, and
$\Delta z_{s-1}(M_{Int,s-1} - t_{Int}) > 0$. (9.2)

$\Delta z_{s-1}\Delta M_{Int,s-1} < 0$ and $\Delta z_{s-1}\Delta M_{VInt,s-1} > 0$. (9.3)

Possible inconsistency which could occur at the FFRs has been all included in Eqs (9). When the lens is moving in the region $[z_2, z_3]$ or $[z_6, z_7]$ toward off focus, it can be detected by Eq. (9.1). Similarly, Eq. (9.2) and (9.3) are designated to check for the inconsistency of lens displacement when it is in the region $[z_1, z_2]$, $[z_5, z_6]$ or $[z_7, z_8]$. When the inconsistency arises, the searching direction will be changed in the next step.

The region $[z_1, z_8]$ determines the depth of interest. It is specified based on the application need. The region $[z_3, z_5]$ denotes the width of NFR which is nothing with the image

features but the magnification of lens and the threshold t_{VAcm}. The values of the parameters z_2, z_6 and z_7 could depend on the image features. However, for a specific LCD structure and under constant illumination, the regional monotones of measures for different image features are very alike. Moderate deviations of the values are tolerable because of the proposed checks of Eqs (8) and (9). By experiment, deviation of z_6 may only moderately affect the focusing speed but not the stability. The proposed checks works even though the regions $[z_1, z_2]$ and $[z_7, z_8]$ are redundant for some specific image features.

It is worth to emphasize that the parameters, z_1 to z_8, are introduced only for conceptual description of the regional monotones of measures. None of the parameter values are required in the proposed focusing algorithm.

As the focusing control overshoots, the stage of rough tuning terminates and the fine tuning starts. The following adaptation of step size will take effects:

$$\Delta z_s = g_3 \, \Delta z_{s-1}, \; g_3 = \begin{cases} g^* & , \; if \; \Delta M_{VAcm} > 0 \\ -g^* & , \; if \; \Delta M_{VAcm} < 0 \end{cases} \text{, and}$$
$$g_3 \geq g_{\min} \qquad (10)$$

where $0 < g^* < 1$; g_3 denotes the step size for fine tuning. It is always a fraction of its previous one. The step size is iteratively reduced, so the stability at the final stage is always guaranteed.

IV. EXPERIMENTAL VERIFICATION

A PC-based AF system was setup for this study [17]. A photo of the system is shown in Fig. 8 where a stepping motor with accuracy of 0.1 μm/step was used to drive the CCD with x50 microscopic lens along the z-axis for focusing control. LCD targets were placed on an x-y table under the lens. Image acquisition rate and resolution were 30 frames/sec and 640 x 480 pixels, respectively. The scope of view was 0.12 mm x 0.09 mm. The DOF of the lens is 2 μm and the width of NFR is about 40 μm.

Experimental tests were executed on a Pentium-IV PC, 3.3 GHz, under the WINDOWS XP environment. The proposed focusing algorithm was implemented in LabVIEW language while computations of FV measures were accomplished by an FPGA processor, Xilinx XSA-3S1000. The FV computations were then transmitted to the PC by RS-232.

The variance measures of Eqs (4) and (6) were computed based on 6x6 sub-windows and each of the sub-windows has a resolution of 60x40 pixels. The resolution was designated based on experimental tests of the repetitive accuracy of $m_{Int,ij}$ and $m_{Acm,ij}$. Under a fair accuracy, lower resolution was used to save the image processing time. Similarly, the number of sub-windows was designated based on tests of the repetitive accuracy of M_{VInt} and M_{VAcm}.

The threshold t_{VAcm} is a critic parameter for designation. For a too small or too large value for it could cause improper switching of use of FV measures that could result in large overshoot or instability of focusing control. In this study, a proper value for it is 0.05 by a designated experiment.

Figure 9 to Fig. 12 show the experimental results of 4 case studies. For each case study, the parameters and gains designated are given in Table 2. The AF tests were run for each case for 100 times. In an AF run, the lens position started at an arbitrary offset from focus. This arbitrary offset was uniformly distributed over the region $[-50\delta, 50\delta]$ and assigned by a random routine.

Conclusions from the above experimental tests are drawn below:

1. Figures 9 and 10 show that a higher value of α at the NFR could result in larger overshooting and takes more time to accomplish the focusing search.
2. Figures 9 and 11 show that a higher value of α at the FFR will result in faster speed. However, inconsistency could occur as it is shown by the non-monotonous trajectories of the focusing control in Fig. 11. The inconsistency can be detected by the proposed inconsistency check and remedied in time.
3. Figures 9 and 12 show that at the FFRs a higher value of γ improves the speed significantly. However, inconsistency becomes more probably to occur as shown by more non-monotonous trajectories of the focusing control in Fig. 12. Again, the necessity of the proposed inconsistency check is justified to ensure the robustness of the control.

The time required for the 100 runs of Case 4 is shown in Fig. 13. It is within 0.6~1.2 sec. In general, the larger the initial offset is, the more the time is required to accomplish the focusing searching. In average, an iteration step takes about 100 ms which includes 40 ms for FPGA processing and RS 232 transmission, 25 ms for the lens displacement, and 35 ms for direction and inconsistency check and computation for step adaptation.

V. CONCLUSIONS

AF for a large depth of lens displacement is studied in this paper. The depth considered in this study is 50 times of the DOF from the focus, and none of a single previous measure is applicable for such a large depth.

An FV method by integrating the measures of the mean of ensemble image intensity, the variance of intensity and ACM over sub-windowing images is proposed. The depth is divided into the regions of NFR and FFR at which the measures have monotones. As given in Eq (7) to Eq. (10), the measures with good sensitivity to image clarity changes at each of the NFRs and FFRs are used to designate rules for adaptation of step size, determination of searching direction, and inconsistency checks.

The initial direction for lens displacement is determined by thresholding. However, a false direction of search can be detected and remedied by the rules in Eqs (8). Adaptation of step size for rough tuning is designated in Eq. (7). The gains for adaptation are scheduled in Table 2 for each of the FFRs,

to boost the speed. The step size for fine tuning is designated in Eq. (10). The gains for adaptation are iteratively reduced, to enhance the stability and accuracy.

Four case studies for the proposed focusing control are illustrated. A response time of 0.6~1.2 sec is achieved. This speed is relatively sufficient for many industrial applications, such as LCD panel laser repairs. One important feature of the proposed method is inclusion of the inconsistency check. As shown in Fig. 11 and Fig. 12, without the inconsistency check, the focusing control could fail with probability of higher than 2%. The concept of integration of regional monotones of measures holds in case the depth of lens displacement needs to be further extended.

ACKNOWLEDGMENT

This work is supported by National Science Council, Taiwan, R.O.C., under the Grand Number NSC 98-2622-E-168-008-CC3.

REFERENCES

[1] Y. Yoshida, S. Shinohara, H. Ikeda, K-I Tada, H. Yoshida, K-I Nishide and M. Sumi, Application of Semiconductor Laser Range Finder to Position Control of Lens in Auto-Focus Camera, IEEE International Conference on Industrial Electronics, Control and Instrumentation, 2357-2361 (1991).

[2] Y. Lee, S.-l. Jang, K. Chung, D. Lee, W. Kim, and C.-W. Lee, A Fuzzy-Control Processor for Automatic Focusing, IEEE Transactions on Consumer Electronics, Vol. 40, No. 2, 138-144 (1994).

[3] F. Li and H. Jin, A Fast Auto Focusing Method for Digital Still Camera, Proceedings of the Fourth International Conference on Machine Learning and Cybernetics, Guangzhou, 18-21, 5001-5005 (2005).

[4] M. J. Chung, Y. H. Yee, W. H. Ann, Development of Compact Camera Module Having Auto Focus Actuator and Mechanical Shutter System for Mobile Phone, Control, Automation and Systems, 17-20, 2319-2322 (2007).

[5] K. Han, X.M. Jiang, Q. Feng and X. C. Zhu, A New Auto-Focusing Method Based on WBDCT for Many Object Situations, Software Engineering, Artificial Intelligence, Networking, and Parallel/Distributed Computing, 481-484 (2008).

[6] K. S. Choi, J. S. Lee, and S. J. Ko, New Autofocusing Technique Using the Frequency Selective Weighted Median Filter for Video Cameras, IEEE Transactions on Consumer Electronics, Vol. 45, No. 3 (1999).

[7] J. T. Huang, C. H. Shen, S. M. Phoong, and H. Chen, Robust Measure of Image Focus in the Wavelet Domain, Intelligent Signal Processing and Communication Systems, 13-16, 157-160 (2005).

[8] S. Y. Lee, S. S. Park, C. S. Kim, Y. Kumar, and S. W. Kim, Low-Power Auto Focus Algorithm Using Modified DCT for the Mobile Phones, Consumer Electronics, 67-68 (2006).

[9] P. T. Yap and P. Raveendran, Image focus measure based on Chebyshev moments**,** Vision, Image and Signal Processing, IEE Proceedings, Vol. 151, Issue 2, 128-136 (2004).

[10] S. H. Jin, J. U. Cho, and J. W. Jeon, FPGA based Passive Auto Focus System Using Adaptive Thresholding, SICE-ICASE, 2290-2295 (2006).

[11] M. Gamadia, N. Kehtarnavaz, and K. Roberts-Hoffman, Low-Light Auto-Focus Enhancement for Digital and Cell-Phone Camera Image Pipelines**,** IEEE Transactions on Consumer Electronics, Vol. 53, Issue 2, 249-257 (2007).

[12] Y. Zhang, Y. Zhang and C. Wen, A New Focus Measure Method Using Moments, Image and Vision Computing, 18, 959-965 (2000).

[13] N. K. C. Nathaniel, P. A. Neow and M. H. Ang Jr., Practical Issues in Pixel-Based Autofocusing for Machine Vision, IEEE International Conference on Robotics & Automation, Seoul, Korea, 21-26, 2791-2796 (2001).

[14] J. He, R. Zhou, Z. Hong, Modified Fast Climbing Search Auto-focus Algorithm with Adaptive Step Size Searching Technique for Digital Camera, IEEE Transactions on Consumer Electronics, Vol. 49, No. 2 (2003).

[15] T. K. Kim, J. S. Sohn , S. H. Lee, K. R. Kwon, and D. G. Kim, Fast Auto-Focus Control Algorithm Using the VCM Hysteresis Compensation in the Mobile Phone Camera**,** Acoustics, Speech and Signal Processing, Vol. 3, III-II, 14-19 (2006).

[16] C. H. Wang, G. Guo, X. Zhang, and P. Ye, A Novel Auto-focusing Method Applied to Micro Manipulation System", ICIRA, Part II, LNAI 5315, 558-565 (2008).

[17] K. C. Lin, On Auto Focusing under a Microscopic View, IEEE International Conference on Industrial Electronics, Control and Instrumentation, 2938-2943 (2007).

Table 1 Thresholding and regional monotones of measures.

	$z_1 \to z_2$	$z_2 \to z_3$	$z_3 \to z_4$	$z_4 \to z_5$	$z_5 \to z_6$	$z_6 \to z_7$	$z_7 \to z_8$
ΔM_{VAcm}	×	×	+	−	×	×	×
$M_{VAcm} \geqq t_{VAcm}$	No	No	Yes	Yes	No	No	No
ΔM_{Int}	+	+	−	+	+	−	−
$M_{Int} \geqq t_{Int}$	No	×	×	×	Yes	×	×
ΔM_{VInt}	−	+	−	+	−	−	+

+ : monotonous increment
− : monotonous decrement
× : not considered

Table 2 Parameters and gains for case studies ($g^* = 0.7$, $t_{VAcm} = 0.05$).

	$z_1 \to z_2$	$z_2 \to z_3$	$z_3 \to z_4$	$z_4 \to z_5$	$z_5 \to z_6$	$z_6 \to z_7$	$z_7 \to z_8$
g_{max}	20	10	6	6	10	15	20
g_{min}	×	×	0.4	0.4	×	×	×
α							
Case 1	2.95	2.85	4.0	4.0	2.85	2.95	3.05
Case 2	2.95	2.85	8.0	8.0	2.85	2.95	3.05
Case 3	3.70	3.60	4.0	4.0	3.60	3.70	3.80
Case 4	2.95	2.85	4.0	4.0	2.85	2.95	3.05
γ							
Case 1	0.2	0.15	1.0	1.0	0.15	0.2	0.25
Case 2	0.2	0.15	1.0	1.0	0.15	0.2	0.25
Case 3	0.2	0.15	1.0	1.0	0.15	0.2	0.25
Case 4	1.2	1.0	1.0	1.0	1.0	1.2	1.4

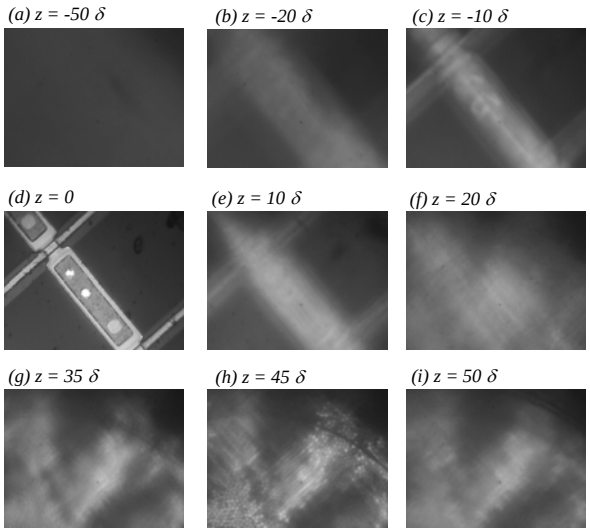

Fig. 1 LCD images under x50 lens views.

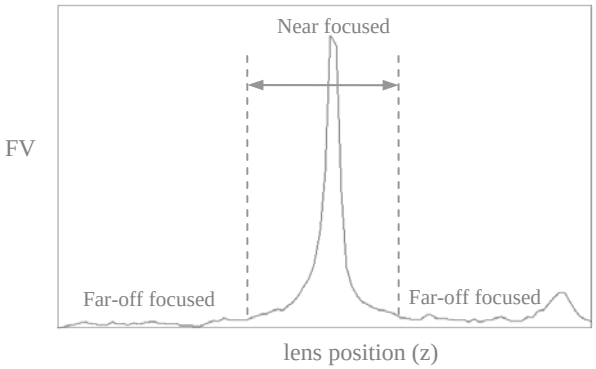

Fig. 2 FV variation for a large depth of lens displacement.

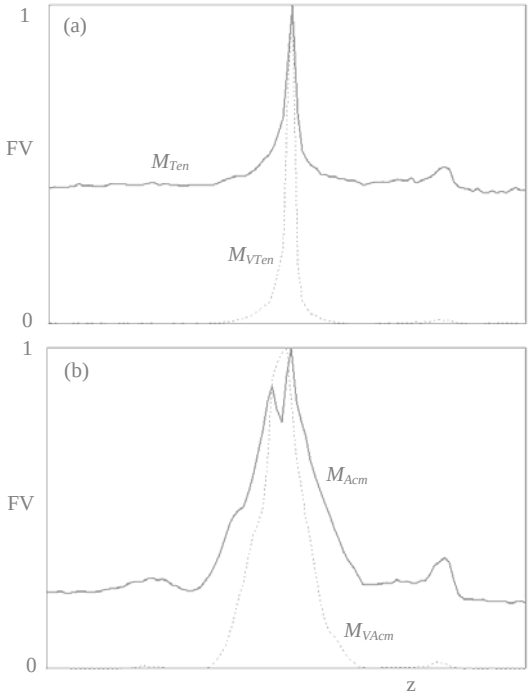

Fig. 3 Previous measures and associate variance measures.

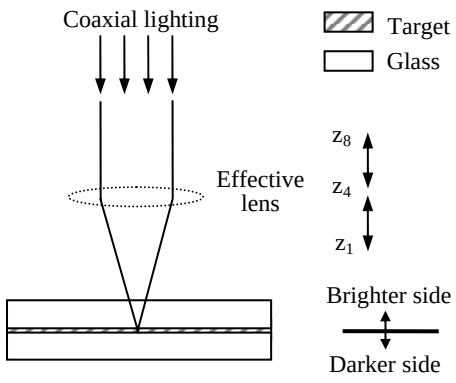

Fig. 4 Schematic of LCD panel under focusing.

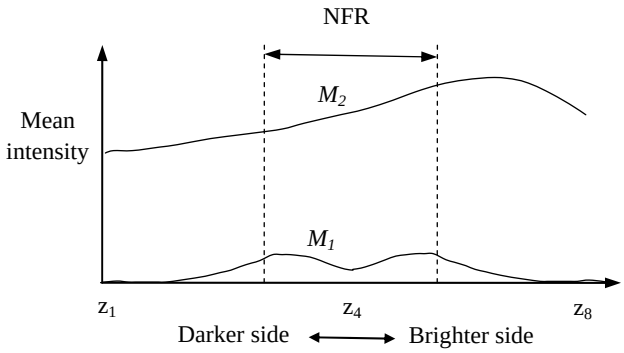

Fig. 5 Two optical mechanisms of the measure M_{int}.

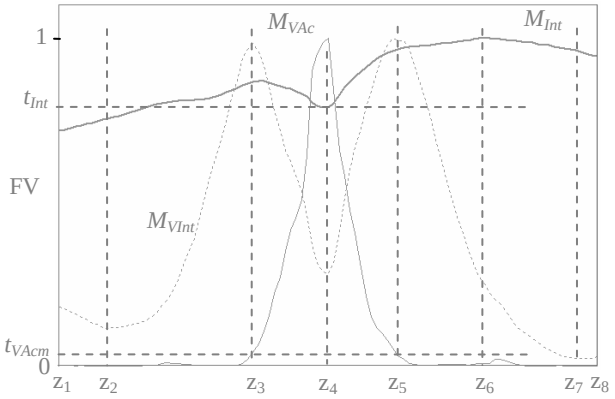

Fig. 6 Thresholding and regional monotones of measures.

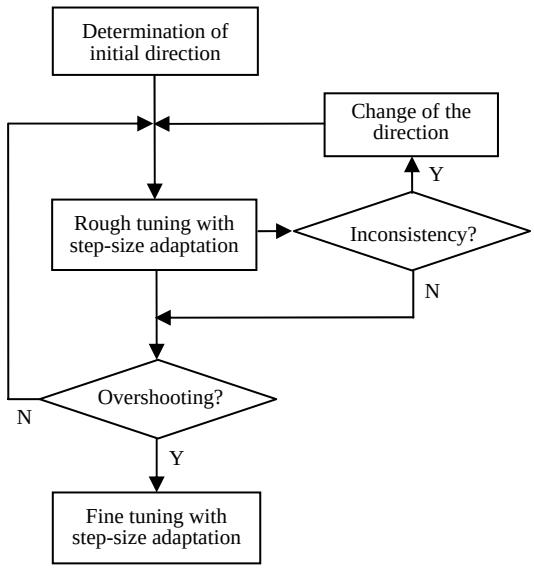

Fig. 7 Flowchart of the proposed focusing control algorithm.

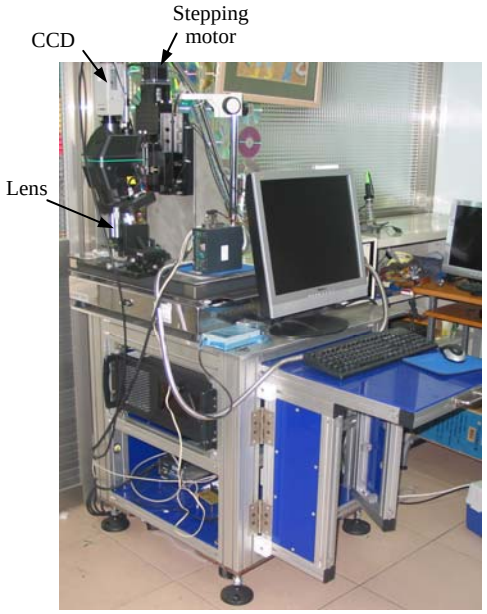

Fig. 8 Photo of the AF system setup for this study.

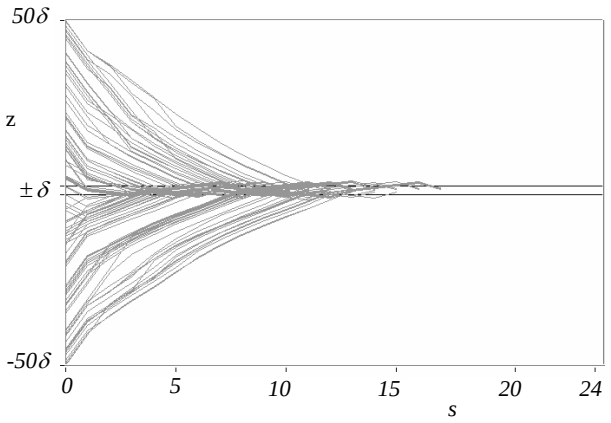

Fig. 9 Experimental results of Case 1.

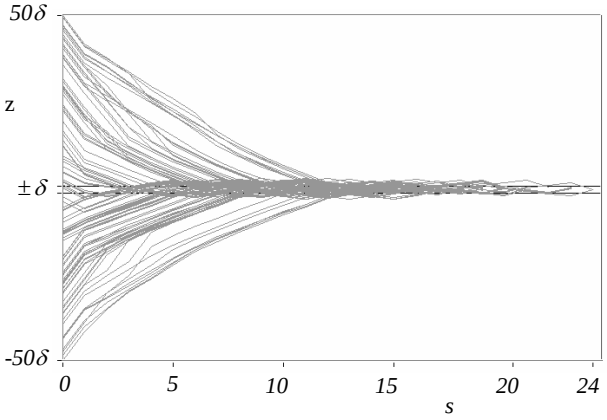

Fig. 10 Experimental results of Case 2.

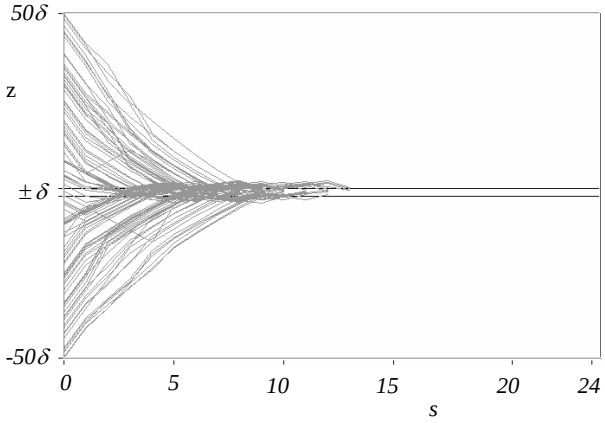

Fig. 11 Experimental results of Case 3.

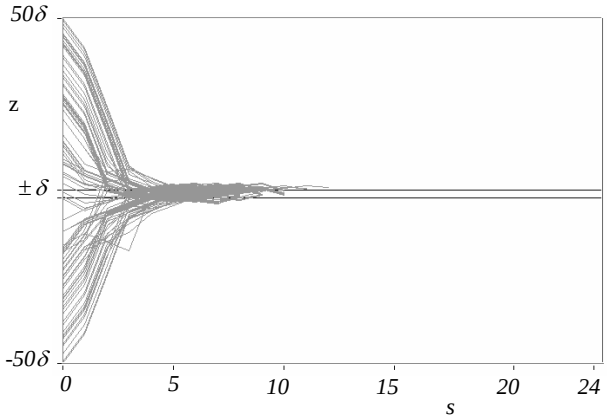

Fig. 12 Experimental results of Case 4.

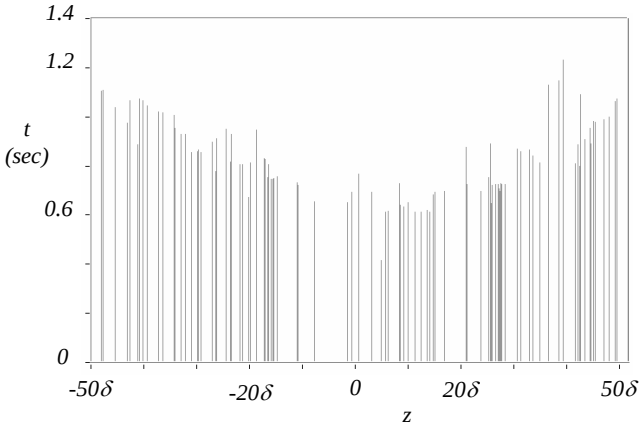

Fig. 13 Time for the focusing control of Case 4.